Featured in Physics

Imaging the Ultrafast Coherent Control of a Skyrmion Crystal

Phoebe Tengdin,[1,*] Benoit Truc,[1,*] Alexey Sapozhnik,[1,*] Lingyao Kong,[2] Nina del Ser,[3] Simone Gargiulo,[1] Ivan Madan,[1] Thomas Schönenberger,[4] Priya R. Baral,[5] Ping Che,[6] Arnaud Magrez,[5] Dirk Grundler,[6,7] Henrik M. Rønnow,[4] Thomas Lagrange,[1] Jiadong Zang,[3,8] Achim Rosch,[3] and Fabrizio Carbone[1,†]

[1]*Institute of Physics, LUMES, École Polytechnique Fédérale de Lausanne (EPFL), Lausanne, Switzerland*
[2]*School of Physics and Optoelectronics Engineering Science, Anhui University, Hefei 230601, China*
[3]*Institute for Theoretical Physics, University of Cologne, Köln, Germany*
[4]*Institute of Physics, LQM, École Polytechnique Fédérale de Lausanne (EPFL), Lausanne, Switzerland*
[5]*Institute of Physics, Crystal Growth Facility, Ecole Polytechnique Fédérale de Lausanne (EPFL), Lausanne, Switzerland*
[6]*Institute of Materials (IMX), Laboratory of Nanoscale Magnetic Materials and Magnonics, Ecole Polytechnique Fédérale de Lausanne (EPFL), Lausanne, Switzerland*
[7]*Institute of Electrical and Micro Engineering, Ecole Polytechnique Fédérale de Lausanne (EPFL), Lausanne, Switzerland*
[8]*Department of Physics and Astronomy, University of New Hampshire, Durham, New Hampshire, USA*

(Received 22 July 2022; revised 13 September 2022; accepted 16 November 2022; published 20 December 2022)

Exotic magnetic textures emerging from the subtle interplay between thermodynamic and topological fluctuation have attracted intense interest due to their potential applications in spintronic devices. Recent advances in electron microscopy enable the imaging of random photogenerated individual skyrmions. However, their deterministic and dynamical manipulation is hampered by the chaotic nature of such fluctuations and the intrinsically irreversible switching between different minima in the magnetic energy landscape. Here, we demonstrate a method to coherently control the rotation of a skyrmion crystal by discrete amounts at speeds which are much faster than previously observed. By employing circularly polarized femtosecond laser pulses with an energy below the band gap of the Mott insulator Cu_2OSeO_3, we excite a collective magnon mode via the inverse Faraday effect. This triggers coherent magnetic oscillations that directly control the rotation of a skyrmion crystal imaged by cryo-Lorentz transmission electron microscopy. The manipulation of topological order via ultrafast laser pulses shown here can be used to engineer fast spin-based logical devices.

DOI: 10.1103/PhysRevX.12.041030

Subject Areas: Condensed Matter Physics, Magnetism
Spintronics

I. INTRODUCTION

When an electron traverses a skyrmion's magnetic structure, the topological ordering causes the electron's spin to pick up a Berry phase. This produces a Lorentz force on the electron as well as a net force on the skyrmion oriented perpendicular to the flow of electric current, known as the Skyrmion Hall effect [1,2]. The effect provides a greatly enhanced coupling of electric current to the magnetic texture, much more efficient than for current-driven manipulation of domain walls [3,4]. In analogy to the case of electric current, skyrmions present in an insulating host material are subject to similar forces when exposed to a pure spin current [5]. However, this process can proceed without the Ohmic losses that exist when using electrical current. Additionally, excitation of spins can be achieved in an ultrafast and contact-free manner using ultrafast lasers on femtosecond timescales [6,7].

The emergence of Cu_2OSeO_3 as a skyrmion hosting Mott insulating material with multiferroic properties and bulk Dzyaloshinskii-Moriya interaction opens the possibility to study and manipulate topological order and skyrmion dynamics purely under the influence of magnetic excitations or electric fields [8]. Additionally, spin currents and collective oscillations in Cu_2OSeO_3 are shown to have an exceptionally low damping and correspondingly long mean free path, making them effective candidates for manipulating spin order [9,10]. Recent works demonstrate the ability to rotate the skyrmion crystal in Cu_2OSeO_3 via thermally generated spin currents [11,12], electric fields

*These authors contributed equally to this work.
†fabrizio.carbone@epfl.ch

[13,14], and a magnetic field gradient in doped crystals [15]. In Refs. [11,12], the spin currents are induced via the spin Seebeck effect with a strong local heat gradient generated from a high-power electron beam. For all previous experiments of this kind, the rotation proceeds on the timescale of hundreds of milliseconds to seconds. To increase the speed of these processes, faster excitation mechanisms are required.

Recent experiments show that circularly polarized femtosecond pulses of light can induce an effective magnetic field of up to 0.6 T in a material for timescales as short as 50–100 fs and drive switching of the magnetic order via the inverse Faraday effect [16–18]. Femtosecond light pulses can also generate spin excitations that have pulse widths in the femtosecond timescale and can travel up to ballistic speeds [19–23], and single pulses are used to trigger the generation of skyrmions in a ferromagnetic or helical background [24,25]. However, the microscopic details of spin excitation on ultrafast timescales are still not fully understood. Experiments investigating these excitations are ultimately constrained by a limited ability to directly image spins on the relevant length (nanometer) and time (femtosecond) scales and are furthermore limited by the inherently irreversible nature of many of the magnetic phenomena studied. The development of Lorentz force microscopy for imaging magnetic textures such as skyrmions coupled with ultrafast excitation of these structures constitutes a promising tool for enhancing the understanding of these spin excitations and their propagation.

In this work, we take advantage of the strong coupling between topological ordering and collective spin oscillations in Cu_2OSeO_3 to drive skyrmion rotational motion with single femtosecond pulses of circularly polarized near-infrared light. After each individual laser pulse, we image the skyrmion crystal in real space via *in situ* cryo-Lorentz force transmission electron microscopy (LTEM). We show that with each laser pulse we rotate the skyrmion crystal by a controlled and irreversible amount. The magnitude of the rotation depends sensitively upon the polarization and fluence of the pulse. With time-varied double pulse measurements performed at the fluence threshold of the observed rotation, we show that this rotation process is driven by a collective magnon excitation that has a characteristic excitation period of approximately 175 ps. Furthermore, the rotation can be switched on and off in a coherent manner by changing the delay time between successive driving pulses with the appropriate polarization. Our conceptually new experimental protocol provides nanoscale images of irreversible modification of the skyrmion crystal orientation that correspond to picosecond dynamics in the material. Through real-space analysis of our images, we generate detailed mappings of the rotations present over macroscopic distances (tens of microns) with a precision that is limited only by the natural length scale of the skyrmions themselves (approximately 60 nm). Additionally, the energy of the light used for excitation (1 eV) is far beneath the band gap of the skyrmion host material, and, thus, control can be achieved with remarkably low values of absorbed fluence, potentially enabling future ultrafast and highly efficient devices.

II. EXPERIMENTAL RESULTS

Figures 1(a) and 1(b) show real-space cryo-LTEM underfocused images of the skyrmion crystal in Cu_2OSeO_3 discussed in this work. Figure 1(a) shows a

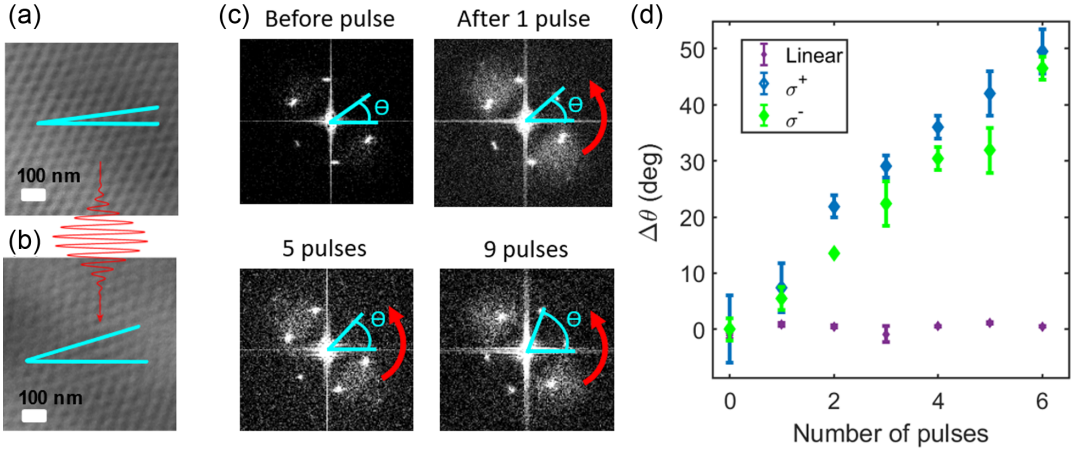

FIG. 1. Illustration and schematic of laser-driven skyrmion crystal rotation process. (a) Real-space images of skyrmion crystal in Cu_2OSeO_3 taken before excitation with the laser pulse and (b) after six successive near-infrared laser pulses each rotate the skyrmion crystal by a discrete amount. Note that the angle (depicted in blue) to the horizontal changes. (c) Fourier transforms of LTEM images following successive pulses of 8 mJ/cm^2 of near-infrared femtosecond laser excitation. The angle of the hexagonal ordering of the skyrmion crystal changes as a function of the number of pulses applied to the sample. (d) Tracking the position of a single peak in the FT of an image while pumping the sample with individual femtosecond laser pulses. Note that σ^+ and σ^- polarizations both rotate the skyrmion crystal in the same direction, while linear polarization does not rotate the skyrmion crystal. The error bars are 95% confidence intervals calculated from the data and multiplied by an uncertainty factor determined from the noise level in the data.

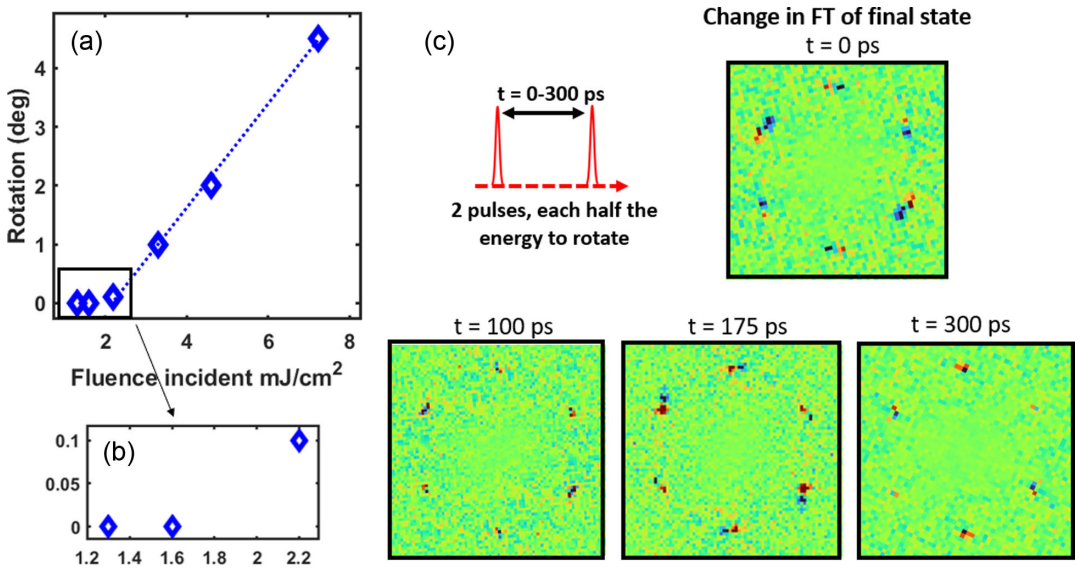

FIG. 2. Fluence and time dependence of skyrmion crystal rotation. (a) Fluence dependence of skyrmion crystal rotation. The dashed line is a linear fit to the data points with fluences from 1.6 to 8 mJ/cm^2. (b) Threshold value of fluence needed to drive rotation in the skyrmion crystal. This value of fluence (2.2 mJ/cm^2) is split into two pulses and used to perform the double pulse time-resolved experiments described in (c). Two laser pulses, each with a fluence of 1.1 mJ/cm^2, are separated by a controlled delay. After the pulses excite the sample, a Lorentz image of the magnetization is recorded. The change in the Fourier transform of the images is shown for various time delays between pulses, illustrating that this time delay between the two pulses directly influences the observed rotation. For clarity, the observed changes are shown after the rotation is driven by 120 pairs of pulses.

metastable skyrmion crystal that forms when we cool the thin lamella from above the Curie temperature (approximately 60 K) to 5 K under an applied magnetic field of 34 mT. Further details of the complete phase diagram of the sample are provided in Supplemental Material [26]. Next, we irradiate the sample with individual femtosecond laser pulses having a waist much larger than the sample size (see Appendix A 1), after which we observe that the skyrmion crystal rotates. Figure 1(c) illustrates our procedure for tracking the rotation of the skyrmion crystal in the real-space TEM images. After each successive laser pulse, we take an image and then take the Fourier transform (FT) of the real-space image (or a subsection of an image) and calculate the angle of the FT in a polar coordinate system. We repeat this process, allowing us to map the change in the angle of the skyrmion crystal following a train of pulses of near-infrared radiation. Further details about the pulse train and imaging settings are given in Appendix A 1. In Fig. 1(d), we extract and plot the angle of a single peak in the FT of the skyrmion crystal after illuminating the sample with femtosecond pulses of light. For the circularly polarized light (both σ^+ and σ^-), each pulse rotates the skyrmion crystal by a discrete amount, with the direction of rotation being the same for both handednesses of polarization, while the linearly polarized light does not rotate the skyrmion crystal. This difference between the rotation of linear and circular polarizations implies that the circularly polarized pulses can drive excitation of magnons (the quanta of spin current) on ultrafast timescales. The mechanism for this excitation is known to be inverse Faraday effect [27] and is discussed later in the text.

In Fig. 2(a), we plot the fluence dependence of the rotation process. We observe that the magnitude of rotation depends sensitively on the amount of laser fluence used in the experiment. In Fig. 2(b), we show that the threshold fluence needed to rotate the skyrmion crystal with circularly polarized light is >1.6 mJ/cm^2. Above this threshold, the rotation amount proceeds in a roughly linear fashion until 8 mJ/cm^2. We observe that pulses with energies above this value (approximately 10 mJ/cm^2) can melt and reform the skyrmion crystal; thus, they cannot be used to rotate the crystal in a controlled way.

Following this fluence dependence, we study the threshold between rotation and nonrotation using a time-resolved technique. We split the photoexcitation pulse into two parts with equal value, and we measure the rotation of the skyrmion crystal as a function of the time delay between the two pulses, each with a fluence of 1.1 mJ/cm^2, corresponding to half of the required fluence for the skyrmion crystal rotation. When the pulses are combined into one pulse at time zero, the excitation is above the threshold where rotation occurs [see Fig. 2(a)]. In Fig. 2(c), we plot the difference in the Fourier transform of two images: one image taken before and one taken after two pulses are sent at the intervals indicated (0–300 ps). We observe that rotation occurs only when the pulses are sent at certain intervals.

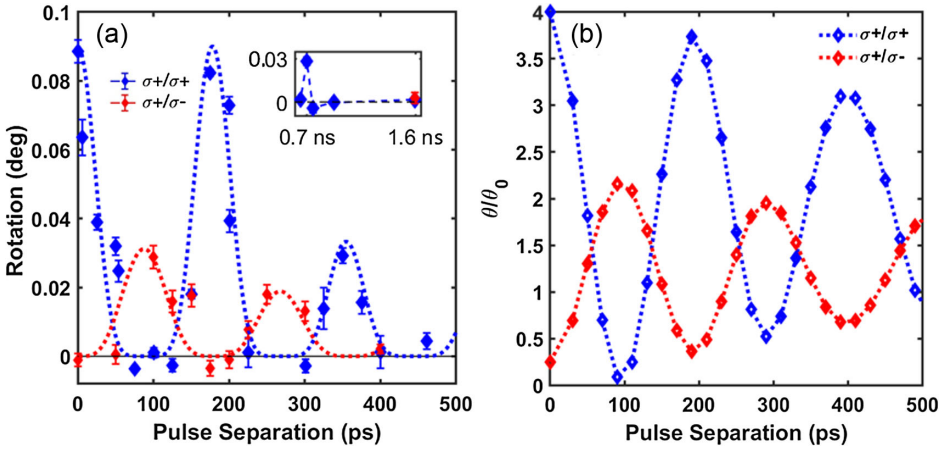

FIG. 3. Detailed time dependence of skyrmion crystal rotation. (a) Double pulse timed experiments showing the rotation of the skyrmion crystal observed as a function of the delay between the two pump pulses. The pulses either have both σ^+ polarization (blue points) or a sequence of σ^+/σ^- polarization (red points). For the blue points, we use pulses of equal amplitude (each with 1.1 $\mathrm{mJ/cm^2}$) and observe a coherent oscillation in the amplitude of rotation with a period of 175 ps that damps out progressively over a nanosecond. For the case of σ^+/σ^- polarization, the second pulse of σ^- polarization has half the amplitude (0.6 $\mathrm{mJ/cm^2}$) of the first one (1.1 $\mathrm{mJ/cm^2}$ with σ^+ polarization). Here, we observe rotation with approximately half the amplitude out of phase with the previous oscillation. The blue and red dashed lines are a guide for the eye. Error bars (95% confidence intervals) are within the markers used. (b) Theoretical prediction of the rotation angle θ/θ_0 for such pulse sequences in a clean system where θ_0 is the rotation angle for a single pulse. The theory is based on the calculation of rotational torques arising from breathing-mode oscillations; see Supplemental Material [26].

This result is further investigated in Fig. 3. We plot the detailed time dependence of the skyrmion crystal rotation as a function of the pulse separation in Fig. 3(a). The blue data points are taken for a sequence of two right-handed circular (σ^+) polarized pulses. The time dependence of the rotation phenomenon shows an oscillation with a period of approximately 175 ps and a damping that takes place over the course of a nanosecond. This response can be attributed only to the launching of a coherent collective magnetic oscillation in the skyrmion crystal that drives the rotation process. For the red data points, we send one pulse with σ^+ polarization and a second pulse with left-handed circular polarization (σ^-) and slightly more than half the fluence value of the first pulse (0.6 $\mathrm{mJ/cm^2}$). For a sequence of $\sigma^+ + \sigma^-$ pulses, we observe a coherent drive that is out of phase with the $\sigma^+ + \sigma^+$ sequence by 180° (approximately 87 ps). This is due to the polarization of the second pulse, which can excite a magnetic field with opposite direction to the first one via the inverse Faraday effect. The magnitude of the rotation also has a weaker amplitude due to the weaker amplitude of the second pulse, showing that the process roughly scales linearly as predicted in Figs. 2(a) and 2(b).

Next, we present a theoretical model that can help us to understand the origin of the collective excitation observed. We compute and show theoretically in Supplemental Material [26] that the combination of Gilbert damping, or another source of damping (e.g., disorder), and breathing-mode oscillations naturally leads to rotational torques, $T^R_{\alpha,\mathrm{pump}} = -\alpha m_0 \int d^3\vec{r}(d\hat{n}/d\theta)\partial_t\hat{n} \propto (\delta M)^2$, where m_0 is the spin density, here we consider only Gilbert damping α, $\hat{n}$ the direction of the magnetization, and $d\hat{n}/d\theta$ the change of the magnetization as a function of the rotation angle θ. For a clean system, we compute the rotation angle $\Delta\theta_{\alpha,\mathrm{pump}}$ after a field pulse of amplitude δB and duration τ and obtain (see Supplemental Material [26])

$$\Delta\theta_{\alpha,\mathrm{pump}} \approx \gamma_{\alpha,\mathrm{pump}} \frac{1}{\alpha N_S}\left(\frac{\delta B}{B_0}\right)^2\left(\frac{\tau}{T_0}\right)^2, \qquad (1)$$

where T_0 is the period of the breathing mode, B_0 the static external magnetic field, N_S the number of skyrmions involved in the rotation, and $\gamma_{\alpha,\mathrm{pump}} \approx 9.7°$ a prefactor for a single pulse which we determine using numerical simulations; see Supplemental Material [26]. For a sequence of two pulses with relative delay time $\Delta\tau$, we show in Fig. 3(b) how the rotation angle changes as a function of $\Delta\tau$. This qualitatively reproduces the experimental result in Fig. 3(a). The remarkable match in the timescales of the experimental and theoretical data confirms that rotational torques induced by the breathing mode can explain our experiment.

Further analysis of our system shows that all rotations are well completed within 5 ns. If we assume a rotation timescale of 5–50 ns, we estimate an effective rotation rate of 2×10^8–2×10^7 deg/s; see Supplemental Material [26]. This rotation rate is more than 6 orders of magnitude faster than previously reported [11]. If we consider the case of coherent control, when the oscillations are stopped after a half period of 87 ps by a pulse of the appropriate amplitude, the effective rotation rate could even be increased to 2×10^{10}.

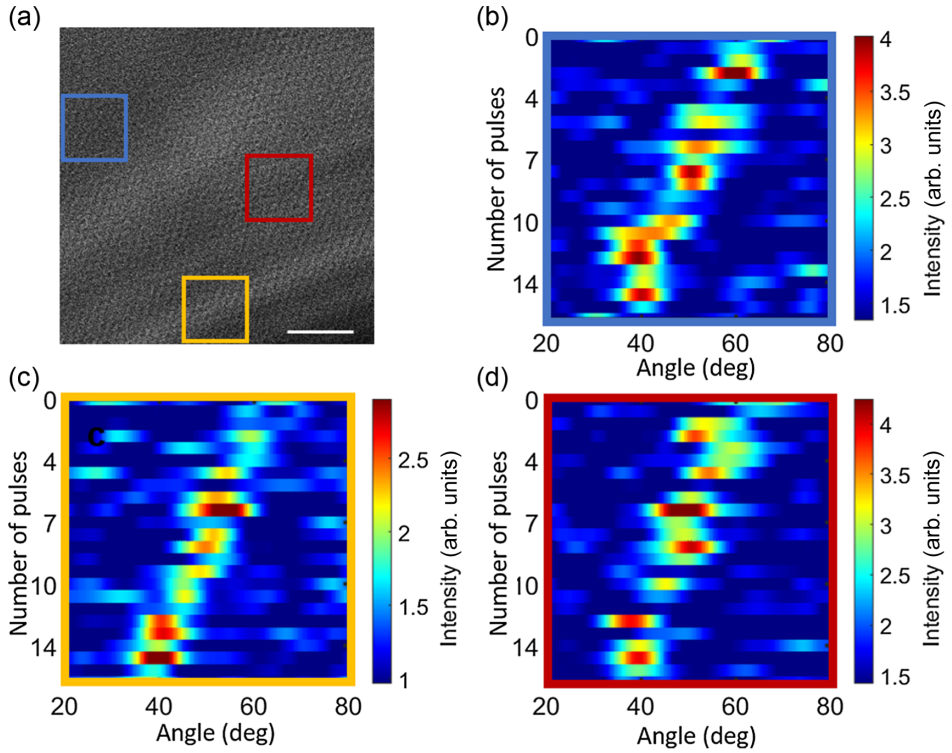

FIG. 4. Skyrmion crystal rotation in a real-space image from the TEM. (a) Real-space LTEM image of the magnetic structure in Cu_2OSeO_3. The scale bar (bottom right) is 500 nm. Response of the skyrmion crystal after excitation by a femtosecond laser pulse train is shown for specific regions of the film in (b)–(d). Each pulse has an energy of 8 mJ/cm^2. We take the FT of each subsection of the image and plot the angle of a single peak in the FT as a function of the number of pulses applied to the sample. The intensity corresponds to the intensity of the peak in the Fourier transform within a region of angles. See Supplemental Material [26] for rotational maps of the entire film.

In Fig. 4, we use our real-space image to map the rotation of the skyrmion crystal across macroscopic distances while again illuminating the sample with a train of femtosecond near-infrared (1 eV) laser pulses. We divide the real-space image in Fig. 4(a) into 25 individual boxes, for each of which we take the FT of the (sub)image and then plot the region around a single point in the FT. In Figs. 4(b)–4(d), we show cutouts of the rotation that takes place in different regions of the sample. See Supplemental Material [26] for additional plots of the rotation present in each subregion of a 5×5 grid of the sample. We find that, by analyzing subregions of the samples, we could better isolate the different regions of the skyrmion rotation, resulting in a higher-quality signal. For the data presented in Fig. 4, the grid size that leads to the best isolation of rotation regions corresponds to an analysis subregion of 460 nm. Since the skyrmion crystal period in this material is approximately 60 nm, this corresponds to a cluster of 7–8 skyrmions across, or approximately 50 skyrmions. We observe rotations as low as 0.05° per pulse in the Fourier transform of our images; here, taken after a sequence of 120 pulses, this corresponds to movements of the skyrmions in real space of about 0.4 nm (per pulse).

III. DISCUSSION

Several mechanisms have previously been identified as potential origins for the rotation of skyrmion crystals. Roughly, they can be grouped into two different classes. The first one is based on a manipulation of anisotropy terms, e.g., by electric fields [13,14], which leads to a rotation by a finite angle. In contrast, a continuous rotation can be induced using the Magnus force imprinted onto the skyrmions by electrical, spin, or heat currents. In an inhomogeneous system, these forces lead to a rotational torque. The inhomogeneity can arise from, e.g., a temperature gradient [4] or simply radial heat currents when the center of the skyrmion crystal is heated [11,12]. While the latter effect may be of relevance in our experiment at high fluence density, the polarization and time dependence of our two-pulse low-fluence experiments in Fig. 3(a) allow us to identify uniquely a new mechanism for the skyrmion rotation.

As shown in Fig. 3(a), the first pulse induces a collective oscillation of the skyrmion crystal with a period of $T = 175$ ps corresponding to a frequency of 5.7 GHz. The origin of these oscillations is already known [16,27]: Via the inverse Faraday effect, the polarized laser light induces an effective magnetic-field pulse which triggers the

breathing mode of the skyrmion crystal, i.e., a coherent oscillation of the size of each skyrmion. The magnetic-field pulse has an amplitude of ± 10 mT for left- or right-polarized light with a duration of $\tau = 50$ fs [16,28]; see Supplemental Material [26] for details. The coherent oscillations are enhanced if the second pulse is either in phase with the same polarization as the first pulse or out of phase with the opposite polarization, as seen for the red data points. Remarkably, the skyrmion rotation starts whenever the amplitude of the breathing-mode oscillation is sufficiently large. This is direct experimental evidence that collective oscillations induced by the inverse Faraday effect lead to rotations of the skyrmion crystal.

Previous numerical and analytical studies [29,30] show that collective magnetic oscillations can induce a translational motion of magnetic textures proportional to δM^2, where δM is the amplitude of the oscillatory mode. In the current setting, such a translational motion is prohibited by symmetry. Quantitatively, however, Eq. (1) predicts—for a clean system and using the ultrashort pulse duration of our experiment—rotation angles about 6 orders of magnitude smaller than observed experimentally; see Supplemental Material [26]. This shows that the Gilbert damping is probably *not* the primary source of the rotational torques. Instead, the rotational torques are most likely induced because the breathing mode triggers a ratchetlike motion in the disorder potential of our sample. Disorder is furthermore responsible for the fact that the rotation angle is not proportional to δB^2, instead following the typical threshold behavior [see Fig. 2(b)] expected for a disorder-pinned system. As the system is in a regime where pinning effects are much more important than effects from the very weak Gilbert damping, it is not surprising that disorder leads to substantially larger rotational torques than predicted for a clean system. As the forces from disorder are many orders of magnitude larger than the forces for damping ($\alpha \sim 10^{-4}$), it is highly plausible that many orders of magnitude larger rotational torques can arise from a disorder mechanism. This is also consistent with the numerical observation in Ref. [31] that boundaries can strongly enhance the ratchetlike motion of skyrmions in oscillating magnetic fields.

In conclusion, our experiment shows that single ultrafast laser pulses can trigger remarkably large rotations of skyrmions using rotational torques induced by collective spin oscillations and a ratchetlike motion in a disordered system. We show that fluence, polarization, and timing can directly control the rotation, while other parameters such as the beam shape have not yet been explored. To modify the spin currents and operate spin-based devices, we could imagine using spatially varied laser beam profiles such as Laguerre-Gaussian beams to generate tailored device frameworks as needed for logical operations. Tightly focusing these beams may also offer the possibility to generate individual skyrmions, as shown in Ref. [32], while the orbital angular momentum in the beams may lead to even more efficient rotations [33,34]. Thus, our work offers the possibility to design new modifiable spintronic devices with logical bit sizes limited only by the spatial pattern of the light used for excitation and with temporal command sequences that can be modified on picosecond timescales. This demonstration of picosecond control over nanometer-scaled topological magnetic objects will lead to an array of new device physics and allow scientists to build new functionalities for skyrmions.

All data, code, and materials used in the analyses are available to readers on request.

ACKNOWLEDGMENTS

We acknowledge useful discussions with Ido Kaminer. We acknowledge support from the ERC consolidator grant ISCQuM and SNSF via sinergia nanoskyrmionics Grant No. 171003, the Humboldt Foundation, the DFG via SPP 2137 (Project No. 403505545) and Collaborative Research Center (CRC) 1238 359 (Project No. 277146847, subproject C04) and CRC 183 (Project No. 277101999, subproject A01), U.S. Department of Energy, Office of Basic Energy Sciences under Grant No. DE-SC0020221, the National Natural Science Foundation of China under Grant No. 11974021, and the SMART-electron project that has received funding from the European Union's Horizon 2020 Research and Innovation Program under Grant Agreement No. 964591. S. G. acknowledges support from Google Inc.

The authors declare no competing interests.

Conceptualization, P. T., B. T., A. S., and F. C.; data analysis, B. T.; experimental methodology, P. T., B. T., A. S., I. M., and T. L.; experimental investigation, P. T., B. T., and A. S.; visualization, P. T., B. T., A. S., and T. L.; sample preparation, T. S., P. B., P. C., and A. M.; theory and simulations, L. K., N.d.S., S. G., J. Z., and A. R.; supervision, A. M., D. G., J. Z., A. R., T. L., and F. C.; writing (original draft), P. T.; writing (review and editing), P. T., B. T., A. S., S. G., P. C., A. M., D. G., H. K., T. L., J. Z., A. R., and F. C.

APPENDIX: METHODS AND MATERIALS

1. Methods: Details of the experimental setup

The experiments are carried out in a modified JEOL JEM2100 TEM [35]. In this instrument, *in situ* cryo-LTEM can be performed in the Fresnel configuration [36] at camera-rate temporal resolution (ms) using a continuous wave electron beam generated thermionically, upon *in situ* pulsed optical excitation of the specimen with a tunable femtosecond source. The camera used for the detection of the electrons is a Gatan® K2 direct detection camera. The sample is cooled to 5 K using a helium-cooled sample holder from Gatan.

A Ti:sapphire regenerative amplifier is used to generate 35-fs pulses of light with a center wavelength at 800 nm and a 34-nm (FWHM) bandwidth. The pulse energy directly from the amplifier is 1.5 mJ per pulse at a 4-kHz repetition rate, and approximately 55% of this light (0.81 mJ) is used to convert to near-IR wavelength via an optical parametric amplifier. After conversion to 1200 nm/1.03 eV, the pulses have the duration of 50 fs, and we use a series of optical choppers to lower the repetition rate to 10 Hz. In this way, we are able to use a mechanical shutter to send individual pulses as desired or to send a train of pulses that has a repetition rate lower than the exposure time of our camera. For the pulse train measurements, the pulses have a repetition rate of either 10 Hz or 10 Hz with every 3rd pulse missing (to check for stability). The camera rate is 20 Hz. For the time-resolved measurements, pairs of pulses are either sent individually or at 4-Hz repetition rate, with total rotation recorded after 120 pulses and the rotation per pulse calculated by dividing the observed rotation angle by 120. The beam is then focused to a diameter of 40 μm (FWHM), which is much larger than the sample size. The magnetic field in the microscope is applied normal to the sample surface along the [111] direction.

2. Materials: Sample preparation

A high-quality single crystal of Cu_2OSeO_3 is grown by the chemical vapor transport method. 25 g of a stoichiometric mixture of CuO and SeO_2 are sealed in a 36-mm-diameter quartz ampule together with 100 mbar of HCl used as transport agent. The ampule is placed in a horizontal two-zone furnace. During the growth, source and sink temperatures are set at 635 °C and 545 °C, respectively. The single crystal is aligned and cut into a cube so that the three main directions correspond to $[1^{-}10]$, [111], and $[^{-}1^{-}12]$, respectively. Then, choosing [111] as the main surface, the cube is cut into slices of approximately 0.5 mm thickness. The sample is thinned to about 110 nm by a focused ion beam technique. The dimensions of the thinned lamella region of the sample are approximately 10 μm × 10 μm × 100 nm.

[1] K. Litzius *et al.*, *Skyrmion Hall Effect Revealed by Direct Time-Resolved X-Ray Microscopy*, Nat. Phys. **13**, 170 (2017).

[2] W. Jiang *et al.*, *Direct Observation of the Skyrmion Hall Effect*, Nat. Phys. **13**, 162 (2017).

[3] J. Grollier, P. Boulenc, V. Cros, A. Hamzić, A. Vaurès, A. Fert, and G. Faini, *Switching a Spin Valve back and forth by Current-Induced Domain Wall Motion*, Appl. Phys. Lett. **83**, 509 (2003).

[4] F. Jonietz *et al.*, *Spin Transfer Torques in* MnSi *at Ultralow Current Densities*, Science **330**, 1648 (2010).

[5] X. Yu *et al.*, *Real-Space Observations of 60-nm Skyrmion Dynamics in an Insulating Magnet under Low Heat Flow*, Nat. Commun. **12**, 5079 (2021).

[6] T. Kampfrath *et al.*, *Terahertz Spin Current Pulses Controlled by Magnetic Heterostructures*, Nat. Nanotechnol. **8**, 256 (2013).

[7] T. Seifert *et al.*, *Efficient Metallic Spintronic Emitters of Ultrabroadband Terahertz Radiation*, Nat. Photonics **10**, 483 (2016).

[8] S. Seki, X. Z. Yu, S. Ishiwata, and Y. Tokura, *Observation of Skyrmions in a Multiferroic Material*, Science **336**, 198 (2012).

[9] N. Prasai *et al.*, *Ballistic Magnon Heat Conduction and Possible Poiseuille Flow in the Helimagnetic Insulator* Cu_2OSeO_3, Phys. Rev. B **95**, 224407 (2017).

[10] I. Stasinopoulos *et al.*, *Low Spin Wave Damping in the Insulating Chiral Magnet* Cu_2OSeO_3, Appl. Phys. Lett. **111**, 032408 (2017).

[11] M. Mochizuki, X. Z. Yu, S. Seki, N. Kanazawa, W. Koshibae, J. Zang, M. Mostovoy, Y. Tokura, and N. Nagaosa, *Thermally Driven Ratchet Motion of a Skyrmion Microcrystal and Topological Magnon Hall Effect*, Nat. Mater. **13**, 241 (2014).

[12] S. Pöllath *et al.*, *Dynamical Defects in Rotating Magnetic Skyrmion Lattices*, Phys. Rev. Lett. **118**, 207205 (2017).

[13] J. S. White *et al.*, *Electric Field Control of the Skyrmion Lattice in* Cu_2OSeO_3, J. Phys. Condens. Matter **24**, 432201 (2012).

[14] J. S. White *et al.*, *Electric-Field-Induced Skyrmion Distortion and Giant Lattice Rotation in the Magnetoelectric Insulator* Cu_2OSeO_3, Phys. Rev. Lett. **113**, 107203 (2014).

[15] M. G. Han *et al.*, *Scaling, Rotation, and Channeling Behavior of Helical and Skyrmion Spin Textures in Thin Films of* Te*-Doped* Cu_2OSeO_3, Sci. Adv. **6**, 1 (2020).

[16] A. V. Kimel, A. Kirilyuk, P. A. Usachev, R. V. Pisarev, A. M. Balbashov, and T. Rasing, *Ultrafast Non-thermal Control of Magnetization by Instantaneous Photomagnetic Pulses*, Nature (London) **435**, 655 (2005).

[17] C. D. Stanciu, F. Hansteen, A. V. Kimel, A. Kirilyuk, A. Tsukamoto, A. Itoh, and Th. Rasing, *All-Optical Magnetic Recording with Circularly Polarized Light*, Phys. Rev. Lett. **99**, 047601 (2007).

[18] F. Hansteen, A. Kimel, A. Kirilyuk, and T. Rasing, *Femtosecond Photomagnetic Switching of Spins in Ferrimagnetic Garnet Films*, Phys. Rev. Lett. **95**, 047402 (2005).

[19] J. Hurst, P.-A. Hervieux, and G. Manfredi, *Spin Current Generation by Ultrafast Laser Pulses in Ferromagnetic Nickel Films*, Phys. Rev. B **97**, 014424 (2018).

[20] A. B. Schmidt, M. Pickel, M. Donath, P. Buczek, A. Ernst, V. P. Zhukov, P. M. Echenique, L. M. Sandratskii, E. V. Chulkov, and M. Weinelt, *Ultrafast Magnon Generation in an Fe Film on* Cu (100), Phys. Rev. Lett. **105**, 197401 (2010).

[21] J. Kimling, G.-M. Choi, J. T. Brangham, T. Matalla-Wagner, T. Huebner, T. Kuschel, F. Yang, and D. G. Cahill, *Picosecond Spin Seebeck Effect*, Phys. Rev. Lett. **118**, 057201 (2017).

[22] A. Alekhin *et al.*, *Femtosecond Spin Current Pulses Generated by the Nonthermal Spin-Dependent Seebeck*

Effect and Interacting with Ferromagnets in Spin Valves, Phys. Rev. Lett. **119**, 017202 (2017).

[23] P. Tengdin *et al.*, *Critical Behavior within 20 fs Drives the Out-of-Equilibrium Laser-Induced Magnetic Phase Transition in Nickel*, Sci. Adv. **4**, eaap9744 (2018).

[24] G. Berruto *et al.*, *Laser-Induced Skyrmion Writing and Erasing in an Ultrafast Cryo-Lorentz Transmission Electron Microscope*, Phys. Rev. Lett. **120**, 117201 (2018).

[25] T. Eggebrecht, M. Möller, J. Gregor Gatzmann, N. R. da Silva, A. Feist, U. Martens, H. Ulrichs, M. Münzenberg, C. Ropers, and S. Schäfer, *Light-Induced Metastable Magnetic Texture Uncovered by In Situ Lorentz Microscopy*, Phys. Rev. Lett. **118**, 097203 (2017).

[26] See Supplemental Material at http://link.aps.org/supplemental/10.1103/PhysRevX.12.041030 for more details.

[27] N. Ogawa, S. Seki, and Y. Tokura, *Ultrafast Optical Excitation of Magnetic Skyrmions*, Sci. Rep. **5**, 9552 (2015).

[28] J. P. Van Der Ziel, P. S. Pershan, and L. D. Malmstrom, *Optically-Induced Magnetization Resulting from the Inverse Faraday Effect*, Phys. Rev. Lett. **15**, 190 (1965).

[29] C. Schütte and M. Garst, *Magnon-Skyrmion Scattering in Chiral Magnets*, Phys. Rev. B **90**, 094423 (2014).

[30] N. del Ser, L. Heinen, and A. Rosch, *Archimedean Screw in Driven Chiral Magnets,*, SciPost Phys. **11**, 009 (2021).

[31] W. Chen, L. Liu, and Y. Zheng, *Ultrafast Ratchet Dynamics of Skyrmions by Defect Engineering in Materials with Poor Conductivity under Gigahertz Magnetic Fields*, Phys. Rev. Appl. **14**, 064014 (2020).

[32] H. Fujita and M. Sato, *Ultrafast Generation of Skyrmionic Defects with Vortex Beams: Printing Laser Profiles on Magnets*, Phys. Rev. B **95**, 054421 (2017).

[33] S. Ali, J. R. Davies, and J. T. Mendonca, *Inverse Faraday Effect with Linearly Polarized Laser Pulses*, Phys. Rev. Lett. **105**, 035001 (2010).

[34] W. Yang, H. Yang, Y. Cao, and P. Yan, *Photonic Orbital Angular Momentum Transfer and Magnetic Skyrmion Rotation*, Opt. Express **26**, 8778 (2018).

[35] L. Piazza, D. J. Masiel, T. Lagrange, B. W. Reed, B. Barwick, and F. Carbone, *Design and Implementation of a fs-Resolved Transmission Electron Microscope Based on Thermionic Gun Technology*, Chem. Phys. **423**, 79 (2013).

[36] S. McVitie and M. Cushley, *Quantitative Fresnel Lorentz Microscopy and the Transport of Intensity Equation*, Ultramicroscopy **106**, 423 (2006).